Journal of the European Ceramic Society **18** (1998) 891–899

PII: S0955-22197-002173
0955-2219/98/$19.00 + 0.00

Strength/Crack-Size Relationship for Knoop-Indented Bending Specimens and Its Application to Silicon Nitride Ceramics

Jianghong Gong[a]* and Zhenduo Guan[b]

[a]Department of Physics, Beijing Normal University, Beijing 100875, People's Republic of China
[b]Department of Materials Science and Engineering, Tsinghua University, Beijing 100084, People's Republic of China

(Received 28 July 1997; accepted 20 November 1997)

Abstract

With a detailed theoretical analysis, a linear relationship is predicted to exist between the fracture strength, σ_f, and the inverse square root of flaw depth, $(1/a)^{1/2}$, of Knoop-indented bending specimens. The effects of residual stresses can be described with a strength revisionary term of the fitted $\sigma_f \sim (1/a)^{1/2}$ equation, while the fracture toughness can be determined directly from the slope term. These predictions are then verified by a variety of tests employed with a pressureless sintered silicon nitride. Variations of the residual stresses in Knoop-indented specimens with annealing temperature are also explored. It is shown that annealing may not be an effective method for eliminating the residual stresses in Knoop-indented bending specimens.

1 Introduction

Indentation fracture has been well-established as an important technique for studying mechanical behavior of brittle glasses and ceramics.[1–5] In this technique, a surface flaw of controlled size and shape is introduced into a mechanical test specimen by conventional microhardness indentation. This flaw initiates fracture during a subsequent breaking test because it is the worst flaw in the specimen. The resultant fracture may then be analyzed to derived fracture mechanics parameters such as fracture toughness. The two major indenter geometries used to produce microcracks are Knoop and Vickers configurations since they are commercially supplied for microhardness testing.[6,7]

More important applications of this technique stem from the analysis of elastic/plastic indentation fracture.[8–12] The indentation analysis is based on the observation that a residual stress, which results from the mismatch between the plastic zone beneath the indentation and the surrounding elastic matrix, dominates both the evolution of the cracks during contact and the response of the cracks to an applied stress during a subsequent breaking testing. The Vickers geometry has been employed in the experimental verifications of this analysis, because the resultant deformation/fracture geometry appears to conform the main simplifying assumption of the analysis.[6] As a result, the mechanics of failure from Vickers indentation-induced microcracks under the combined influences of residual stress and a normal applied tension has been analyzed in detail.[13–15] However, similar studies have rarely been conducted for the Knoop geometry, although the elongated Knoop indenter, which generates a single semi-elliptical surface flaw, appears to be more suitable for certain applications in the evaluations of ceramics.[6,7] The applications of Knoop indentation are thus limited by the unknown influence of the residual stress on fracture. In order to eliminate some of the uncertainty associated with the residual stress about Knoop indentation, annealing was usually conducted on Knoop-indented specimens before breaking test in the previous studies.[16–18]

In the present study, a fracture-strength/crack-size function is presented to quantify the response of Knoop indentation-induced surface flaw to an applied stress by incorporating the residual stresses in the fracture mechanics analysis. Two kinds of residual stresses are considered in this study: one is the indentation residual stress mentioned above and the other is the residual surface stress which is

*To whom correspondence should be addressed at: Laboratoire de Physique des Matériaux, Ecole des Mines de Nancy, Parc de Saurupt, 54042 Nancy Cedex, France.

introduced during the surface treatments of specimens, such as grinding[19–21] and tempering.[13] The predicted function is then verified, with particular emphasis on exploring the efficacy of annealing for eliminating the effects of residual stresses, with a series of experiments, which are conducted with Knoop-indented bending specimens of silicon nitride ceramic.

2 Theoretical Background

A diagram of a bending specimen having a surface flaw of the type introduced by a single Knoop microhardness indentation is shown in Fig. 1. According to fracture mechanics considerations, the flaw will propagate catastrophically when the stress intensity, K_I, reaches a critical value, K_{IC}. For the general case, the stress intensity for the semi-elliptical surface flaw shown in Fig. 1 may be given by:[13]

$$K_I = K_a + K_r + K_s \tag{1}$$

where K_a, K_r, and K_s represent the contributions from the applied bending stress, the residual stress due to indentation, and the residual stress due to the surface treatments of specimen, respectively.

2.1 Expression for K_a

The widely used expression for K_a in eqn (1) is:[7]

$$K_a = \sigma_a M \sqrt{\frac{\pi a}{Q}} \tag{2}$$

where σ_a is the applied bending stress, a the flaw depth, M the free surface correlation factor, and $Q \approx \phi^2$ for the brittle ceramics. The term ϕ, a complete elliptical integral of the second kind, is given by:

$$\Phi = \int_0^{\pi/2} \left[\sin^2\theta + \left(\frac{a}{c}\right)^2 \cos^2\theta\right]^{1/2} \mathrm{d}\theta \tag{3}$$

where $2c$ is the flaw length at the free surface.

Experimental observations have shown that, in an appropriate range of indentation load, the ratio of the flaw depth to half-length, a/c, of Knoop indentation-induced flaws is a constant for a given material.[18,22–25] Thus, the flaw shape factor in eqn (2), Q, can be considered as a constant independent of indentation load.

No exact theoretical solution has yet been formulated for the free surface correlation factor, M. The most accurate solutions for M are those of Newman and Raju.[26] According to these solutions, the variation of M with the parameters of importance, including the ratio of flaw depth to half-length, a/c, the ratio of flaw depth to specimen thickness, a/t, and the parametric angle around the flaw periphery, φ, is shown in Fig. 2. Two key features should be noted from Fig. 1: (1) the maximum value of M (and hence K_a) generally occurs at the specimen surface, i.e. $\varphi = 0°$; (2) the effect of a/t ratio on M is insignificant for a given a/c ratio when $\varphi = 0°$. So it is reasonable to treat M as a constant approximately in a limited range of a/t. In fact, M is usually considered as a constant in literature, for the flaw depth to specimen thickness ratio, a/t, usually varies slightly from specimen to specimen.[16,23,25,27]

Based on the discussions above, eqn (2) can be rewritten as

$$K_I = Y_a \sigma_a \sqrt{a} \tag{4}$$

where $Y_a = M\sqrt{\frac{\pi}{Q}}$ is a constant.

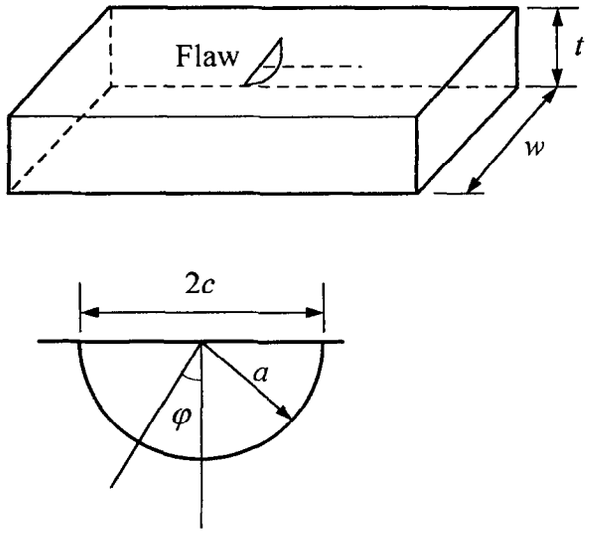

Fig. 1. Schematic view of Knoop indentation-induced flaw in bending specimen.

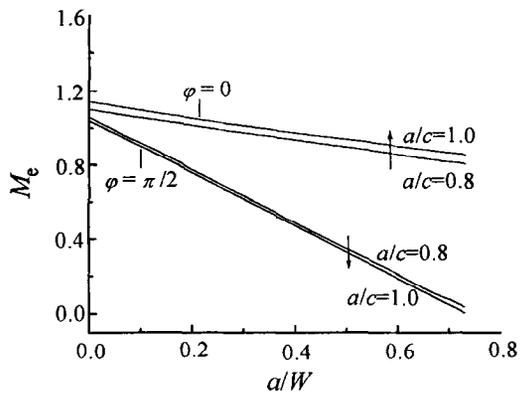

Fig. 2. Solution of Ref. 26 for free-surface correction factor M in bending loading.

2.2 Expression for K_r

Indentation residual stress results from the mismatch between the plastic zone beneath indentation and the surrounding elastic matrix.[9] This kind of residual stress is tensile which acts on the flaw fronts both at the surface and in the interior of the specimen. The basis of formalisms dealing with indentation residual stress effects is to assume that this situation can be approximated by available solution for a center-loaded, penny-shaped crack in an infinite medium.[9,10] This leads to an expression of the form:[7]

$$K_r = \chi_r P/c^{3/2} \tag{5}$$

where P is the indentation load, and χ_r a constant dependent on indenter geometry and the material properties but assumed independent of indentation load.

For Vickers indentation-induced flaws, a constant value of $P/c^{3/2}$ has been observed for a wide variety of materials and eqn (5) is usually used as a basic equation for evaluating material toughness in truly inert environments by equating K_r to K_{IC}.[28] For Knoop configuration, however, K_r usually increases with indentation load.[6,7] The difference between the indentation load/crack length relations for Vickers and Knoop indentations may be considered as a result of the difference in crack profiles between the two configurations.

In general, Vickers indentation always produces cracks emanating from all four diagonal corners for each impression, even at a lower indentation load. However, microcracking due to Knoop indentation is rarely observed on the surface of specimen if a lower indentation load is used,[7] unless an additional surface polishing is done after indentation.[29] Observed on the fracture surface, the Knoop indentation-induced flaw is readily visible to be semi-elliptical;[16–18] whereas the Vickers cracks are proved to be surface-localized radial cracks[30,31] or so-called 'well-developed' median/radial crack systems.[9,10] These observations suggest that the cracking behaviors are rather different for Knoop and Vickers indentations. As a result, a constant value of $P/c^{3/2}$ may not be expected for Knoop configuration produced at a relatively lower load, for little radial cracking can be detected.

Although a distinct difference exists between the cracking behaviors in Knoop and Vickers indentations, eqn (5) should apply to both configurations, according to the detailed analysis by Petrovic.[7] Experimental observations show that the actual length of Knoop indentation-induced flaws, $2c$, is close to the diagonal length of Knoop indentation, d.[7,24,25] Because the value of P/d^2 is a measure of material hardness, a nearly constant value of P/c^2, rather than $P/c^{3/2}$, can be expected. Thus, for Knoop indentation-induced flaw, eqn (5) can be rewritten as:

$$K_r = Y_r\sqrt{a} \tag{6}$$

where $Y_r = \chi_r\left(\frac{P}{c^2}\right)\sqrt{\frac{c}{a}}$ is a constant. Equation (6) shows an evident increase tendency of K_r with indentation flaw depth, a, and hence with indentation load, P.

2.3 Expression for K_s

Another kind of residual stress to be considered here is the residual surface stress caused by grinding, a common processing step of engineering ceramics. Recent studies[20,21] have shown that surface grinding processes, which remove material mechanically, introduce residual stress, which is compressive near the surface and tensile underneath, into the specimens. This residual surface stress acts uniformly over the area of the primary crack, i.e. the indentation flaw, and the appropriate stress intensity, K_a, may be described as:[32]

$$K_s = M\sigma_s\sqrt{\frac{\pi a}{Q}} \tag{7}$$

where σ_s is residual surface stress, M and Q are the same parameters that appeared in eqn (2).

Similarly, eqn (7) can also be written as:

$$K_s = Y_a\sigma_s\sqrt{a} \tag{8}$$

where Y_a is the same parameter that appeared in eqn (4).

The residual surface stress can also be introduced by other surface treatment processes, such as tempering.[13] The contributions from these residual surface stresses to stress intensity have the same form as eqn (8). Defining α_s as the sum of all kinds of residual surface stresses existing on the specimen surface, eqn (8) may then be used to describe the total contributions of the residual surface stresses.

Substituting eqns (5), (6), and (8) into eqn (1) gives:

$$K_I = Y_a(\sigma_a + \sigma_r + \sigma_s)\sqrt{a} \tag{9}$$

where $\sigma_r = Y_r/Y_a$ is defined as an equivalent indentation residual stress.

At critical condition, $K_I = K_{IC}$, $\sigma_a = \sigma_f$, eqn (1) can be rearranged as:

$$\sigma_f + \sigma^* = B\sqrt{\frac{1}{a}} \tag{10}$$

where both $\sigma^* = \sigma_r + \sigma_s$ and $B = K_{IC}/Y_a$ are constants for a given material.

Equation (10) shows that a linear relationship exists between the fracture strength of Knoop-indented bending specimen, σ_f, and the inverse square root of the indentation flaw, $(1/a)^{1/2}$. The effects of residual stresses, including the indentation residual stress and the residual surface stresses, can be described properly with a strength revisionary term appeared in the $\sigma_f \sim (1/a)^{1/2}$ fitting equation, σ^*, while the fracture toughness, K_{IC}, can be determined directly from the slope term. It should be pointed out that the stage of precursor stable growth of indentation flaws before failure under an applied stress, which usually occurs in the crack system produced by Vickers indentation,[6,13,14] should not be considered here, for the main prerequisite for deducing eqn (10), parameters a/c, Y_a, and P/c^2 being constants, have been observed to be satisfied in the critical rather than the initial state.[24,25]

Equation (10) has been applied by the present authors[24,25,33,34] to determine K_{IC} values for some materials and a quite good linear relationship is always observed between σ_f and $(1/a)^{1/2}$. Similar results can also be obtained by analyzing the experimental results presented in a series of works by Govila.[35–37] For example, regression analysis by a linear least square fit of eqn (10) with the data listed in Table II of Ref. 37 gives:

$$\sigma_f + 152{\cdot}23 = 5{\cdot}43\sqrt{\frac{1}{a}}$$

This relationship has a good correlation factor, 0·98, and there is an evident strength revisionary term appearing in the left side of this expression.

3 Experimental

The material selected for this study is a pressureless sintered silicon nitride. Test specimens are 36 mm long×4 mm wide×3 mm thick, approximately. All surfaces of specimens are ground lengthwise and the edges chamfered to prevent notch effects. The tensile surface of specimen is carefully ground and polished to a 0·5 μm diamond paste finish.

Specimens are then divided into 13 samples, each sample containing six specimens. Three series of experiments are conducted with these samples. While the series A experiments are performed immediately after precracking, the specimens used in the series B and C experiments are annealed at elevated temperatures before and after precracked, respectively. The details of these series of experiments are given in Table 1. In these experiments, precracking of specimens is done with a Knoop microhardness tester with loads ranging from 20 to 45 N. Different loads are selected for the precracking of different specimens in the same sample, in order to make the flaw depth vary from specimen to specimen. All flaws are carefully placed in the center of the tensile surface in an orientation perpendicular to the tensile stress direction. Annealing is conducted in air. No preload is applied on test specimens during annealing. All specimens are broken at room temperature in 4-point bending with a crosshead speed of 0·05 mm min^{-1}. The outer and inner knife edges of the testing fixture are spaced 30 mm and 10 mm, respectively. The flaw dimensions, a and $2c$, on the fracture surface of specimen are then measured carefully using optical microscopy, with a magnification of 120 and an error of measurement of ± 1 μm.

Table 1. Summary of the details of experimental procedures

Series	*Sample denotation*	*Details of the experimental procedure*
A	A0	Precracked, and broken
B	B1	Annealed at 700°C for 1 h, precracked, and broken
	B2	Annealed at 800°C for 1 h, precracked, and broken
	B3	Annealed at 900°C for 1 h, precracked, and broken
	B4	Annealed at 950°C for 1 h, precracked, and broken
	B5	Annealed at 1000°C for 1 h, precracked, and broken
	B6	Annealed at 1100°C for 1 h, precracked, and broken
	B7	Annealed at 1200°C for 1 h, precracked, and broken
C	C1	Precracked, annealed at 700°C for 1 h, and broken
	C2	Precracked, annealed at 800°C for 1 h, and broken
	C3	Precracked, annealed at 900°C for 1 h, and broken
	C4	Precracked, annealed at 950°C for 30 min, and broken
	C5	Precracked, annealed at 1000°C for 10 min, and broken

The semi-elliptical contour of the indentation crack can always be detected easily for the material used in the present study. There is no evidence of stable or subcritical crack growth observed on the fracture surfaces of specimens. Similar phenomena have also been observed in Si_3N_4-based ceramics by other authors.[18,29,35] Therefore, there is little difficulty in measuring the crack dimensions accurately on the fracture surface of the specimen.

For the purpose of comparison, the fracture toughness of the test material, K_{IC}, is measured with the conventional single-edge-notched beam (SENB) method and the chevron-notched bending beam (CNB) method,[38] respectively.

4 Results and Discussion

Two key issues should be discussed initially. The first is whether the parameters a/c, Y_a, and P/c^2 can be treated as constants for indented specimens tested under a certain condition. The second is whether eqn (10) can describe the fracture strength/flaw depth relation properly. Clearly, the two issues are the main prerequisites for using eqn (10) to determine the fracture toughness and study the effects of residual stresses in Knoop-indented bending specimens.

Experimental results of sample A0 are given in Table 2. With the increasing indentation load, and hence the flaw depth, both a/c and P/c^2 exhibit a slightly statistical fluctuation around an average of 0·856 and 1·183, respectively, indicating that these two parameters are independent of indentation load. A decreasing tendency is observed in the calculated value of Y_a with the increasing flaw depth. This is due to the variation of the free surface correlation factor, M, with the increasing a/t. Because the standard deviation of the values of Y_a is rather small, it is reasonable to assume that Y_a is also independent of indentation load.

Similar conclusions can also be deduced by analyzing the experimental results of other samples. The values of the average and the standard deviation of a/c, Y_a, and P/c^2 for each sample are calculated and summarized in Table 3.

Figure 3 shows the experimental results on a σ_f versus $(1/a)^{1/2}$ plot. It is clear that a good linear relationship exists between σ_f and $(1/a)^{1/2}$ for each sample. Correlations for these plots are high, $r^2 > 0{\cdot}96$, implying that eqn (10) gives a proper description for the fracture strength/flaw depth relation of Knoop-indented bending specimens. The slope, B, and the intercept, σ^*, for each line in Fig. 3 are evaluated by linear regression and the results are also listed in Table 3.

4.1 Effects of annealing on K_{IC} determination

Knoop-indented bending (KIB) method has been applied previously to measure K_{IC} values for a wide variety of ceramics.[16,17,35] In this method, the residual stresses in the indented specimens are usually assumed to be eliminated completely by annealing at elevated temperatures and the K_{IC} value is calculated with eqn (2). Based on the theoretical consideration mentioned in Section 2, a modified Knoop-indented bending (MKIB) method can be proposed for K_{IC} determination, in which annealing of specimens is not necessary and the K_{IC} value can be determined directly from the slope term of the fitted $\sigma_f \sim (1/a)^{1/2}$ equation, i.e:

$$K_{IC} = BY_a \tag{11}$$

Here we conduct a brief comparison between these two methods. For convenience, we denote the K_{IC} values obtained with the KIB and the MKIB methods as $K_{IC}{}^{K}$ and $K_{IC}{}^{M}$, respectively.

For sample A0, $K_{IC}{}^{M}$ is determined to be 7·01 MPa$\sqrt{m}$. This value is comparable to the value,

Table 2. Results of the series A experiments

Specimen No.	*Indentation load (N)*	*Flaw depth (μm)*	*Flaw length (μm)*	a/c	Y_a	P/c^2 *(GPa)*	*Fracture strength (MPa)*
1	19·6	110	258	0·853	1·278	1·178	460·2
2	24·5	128	294	0·871	1·273	1·134	429·1
3	29·4	136	322	0·845	1·273	1·134	404·0
4	34·4	142	330	0·861	1·270	1·260	399·0
5	29·2	156	364	0·857	1·268	1·183	381·6
6	44·1	162	382	0·848	1·267	1·201	366·1

Table 3. Summary of the experimental results

Sample	a/c	Y_a	P/c^2 *(GPa)*	B $(MPa\sqrt{m})$	σ^a *(MPa)*
A0	0·856 ± 0·009	1·272 ± 0·004	1·183 ± 0·044	5·51	63·62
B1	0·851 ± 0·009	1·270 ± 0·002	1·096 ± 0·037	5·57	72·77
B2	0·845 ± 0·006	1·268 ± 0·004	0·969 ± 0·039	5·54	60·85
B3	0·844 ± 0·007	1·275 ± 0·005	1·492 ± 0·089	5·45	102·97
B4	0·848 ± 0·007	1·277 ± 0·002	1·729 ± 0·045	5·49	138·38
B5	0·847 ± 0·007	1·279 ± 0·001	2·419 ± 0·048	5·40	104·34
B6	0·852 ± 0·004	1·278 ± 0·001	2·949 ± 0·057	4·37	166·91
B7	0·852 ± 0·004	1·280 ± 0·003	2·129 ± 0·057	3·91	146·11
C1	0·844 ± 0·006	1·279 ± 0·002	2·569 ± 0·153	5·52	140·07
C2	0·844 ± 0·010	1·281 ± 0·171	2·246 ± 0·171	5·47	146·88
C3	0·852 ± 0·006	1·281 ± 0·001	3·465 ± 0·071	5·44	92·81
C4	0·850 ± 0·006	1·281 ± 0·003	3·102 ± 0·142	5·46	73·78
C5[a]	~0·854	~1·284	~6·176	~5·25	~37·78

[a]Only two of the six specimens are broken from the site of the indentation flaw.

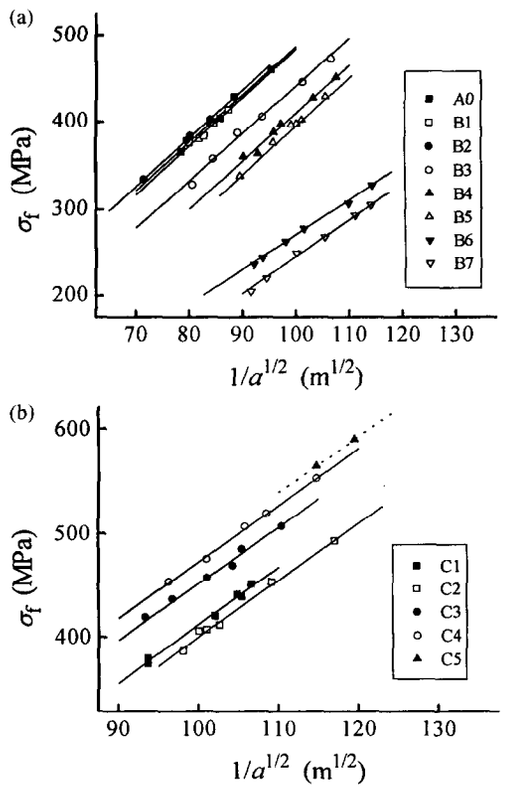

Fig. 3. $\sigma_f \sim (1/a)^{1/2}$ plots obtained from the three series of experiments.

$6{\cdot}8 \pm 0{\cdot}2$, which is measured with CNB method, but lower compared to the value measured with SENB method, $8{\cdot}3 \pm 0{\cdot}2$ MPa$\sqrt{m}$. It is well-known that the conventional SENB method usually gives a relatively higher K_{IC} value due to the blunting effect at the notch-tip.[39,40] Thus, the comparison between these K_{IC} values suggests that the MKIB method seems to be reliable for K_{IC} determination. In fact, this conclusion has been deduced in our previous works.[24,25] $K_{IC}{}^{K}$ value for sample A0 is determined to be $6{\cdot}06 \pm 0{\cdot}10$ MPa$\sqrt{m}$. Clearly, this lower value reflects the influences of the residual stresses.

The K_{IC} values obtained from the series B experiments are shown in Fig. 4, where the abscissa is the temperature at which specimens are subjected to air annealing before precracking. Also shown is the K_{IC} value obtained with the series A experiments. It can be seen that both K_{IC} values obtained with MKIB and KIB methods, K_{IC}^{M} and K_{IC}^{K}, exhibit similar tendency with the increasing annealing temperature. The main reason for the fact that the is always lower than is that the indentation residual stress is not eliminated in this series of experiments, for annealing is conducted *before* precracking. Note that the K_{IC}^{M} value is identical with that obtained from the sample A0 until annealing temperature increases to 1000°C, and then a continuous decrease in K_{IC}^{M} occurs with a further increase in annealing temperature. Because the KMIB method may give a reasonable K_{IC} value, this behavior seems to suggest that annealing at an unsuitable higher temperature may result in a change in material properties. Therefore, a suitable annealing temperature should be selected carefully for the K_{IC} determination with the KIB method.

We now turn to analysis of the K_{IC} values obtained from the series C experiments, which are shown in Fig. 5. In this series, annealing of specimens is conducted after precracking. Since the limitation of annealing temperature for the present material seems to be 1000°C, above which annealing may result in a change in material properties, 1000°C is selected as the highest annealing temperature in this series. It can be concluded from Fig. 5 that annealing at temperatures not higher than 1000°C after precracking also has little effect on K_{IC} measurement with the MKIB method, for the K_{IB}^{M} values for samples C1–C5 are comparable to that for sample A0. The variation of the K_{IC}^{K} with annealing temperature can be considered as a result of the reduction of the residual stresses.[16,17] However, a distinct difference exits between K_{IC}^{K} and K_{IC}^{M} in the whole range of annealing temperature considered, implying an uncompleted elimination of the residual stresses.

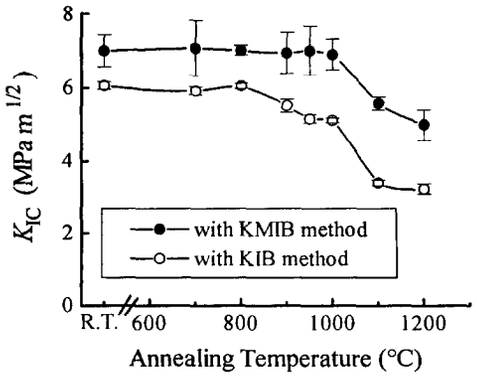

Fig. 4. Effect of annealing before precracked on the K_{IC} values determined with the KIB and MKIB methods.

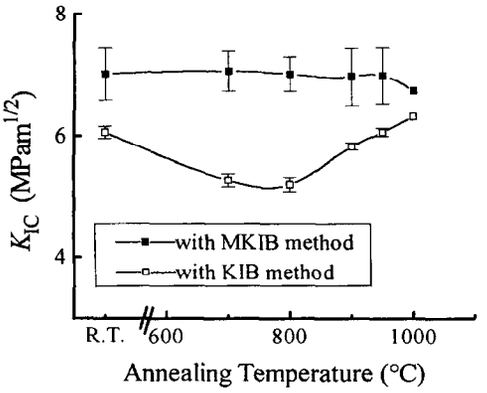

Fig. 5. Effect of annealing after precracked on the K_{IC} values determined with the KIB and MKIB methods.

Flaw healing is always observed on the fracture surface of specimens used in series C experiments, samples C1–C5. Annealed flaws have sizes smaller than that of unannealed flaws. However, no change in the ellipticity of the flaw, i.e. the ratio of flaw depth to half-length, is observed. The extent of flaw healing increases with annealing temperature, resulting in an increasing tendency in the value of P/c^2 (Table 3). Particularly after being annealed at 1000°C, the room temperature fracture of most indented specimens no longer occurs at the site of the indentation flaw. Therefore, crack healing may be another obstacle for using the KIB method to measure fracture toughness.

4.2 Effects of annealing on the residual surface stresses

In series B experiments, the precracking of specimens is conducted after annealing. Therefore, annealing should have no effect on the indentation residual stress and the variation of the values of the strength revisionary term in eqn (10), $\sigma^* = \sigma_r + \sigma_s$, may be related directly to the variation of residual surface stresses, which are caused by the surface treatments of specimens, with annealing temperature in this series.

Figure 6 shows the value of σ^* as a function of annealing temperature for series B experiments. Note that the values of σ^* corresponding to annealing temperatures of 700° and 800°C are close to that obtained from series A experiments, implying that annealing at temperature lower than 800°C has no or little effect on the residual surface stresses. The sudden increase in σ^* after being annealed at 900°C can be interpreted as the onset of appreciable relief of the residual surface stresses, for this kind of stresses is generally compressive near the free surface.[20,21] With a further increase in annealing temperature, σ^* tends to invariable again. This behavior seems to say that the residual surface stresses can be eliminated completely by annealing the specimens at an appropriate temperature.

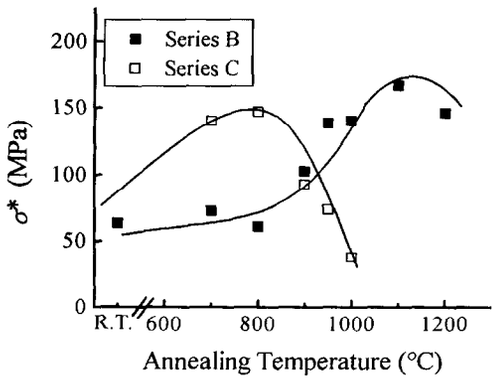

Fig. 6. Effect of annealing on the residual stresses in the indented specimens.

The magnitudes of the residual stresses, σ_s, and the equivalent indentation residual stress, σ_r, can be estimated from the above discussion. Since the residual surface stresses may be eliminated completely after being annealed at 950° and/or 1000°C, the σ^* values obtained from samples B4 and B5 may represent the effects of indentation residual stress in Knoop-indented bending specimens. Thus, the equivalent indentation residual stress can be estimated as:

$$\sigma_r \approx [(\sigma^*)_{B4} + (\sigma^*)_{B5}]/2 \approx 139\text{MPa} \qquad (12)$$

eqn (12) shows that the net effect of indentation residual stress can be equivalent to a tensile stress of about 139 MPa which supplements the applied load during the breaking test.

On the other hand, the total effect of residual stresses in precracked, unannealed specimens is given by the σ^* value obtained from the group A, i.e.

$$\sigma_r + \sigma_s \approx (\sigma^*)_{AO} \approx 64\text{MPa} \qquad (13)$$

Combining eqns (12) and (13), the magnitude of the residual surface stresses in the as-received specimens, σ_s, is determined to be about −75 MPa. The negative value of σ_s indicates that the residual surface stresses are compressive.

The average strength of the unprecracked specimens is measured to be 612 MPa before annealing and 558 MPa after annealed at 1000°C, respectively. The degradation in strength of annealed specimen is due mainly to the relief of the residual surface stresses.[21] The difference between the strength of unprecracked specimens after and before annealing, −54 MPa, is close to the magnitude of the residual surface stresses estimated above, −75 MPa, giving an indirect support for the theoretical considerations in Section 2.

4.3 Effects of annealing on the indentation residual stress

In series C experiments, the precracking of specimens is conducted before annealing. Therefore, annealing may affect both the indentation residual stress and the residual surface stresses.

The values of σ^* for series C experiments are also shown in Fig. 6. Note that σ^* increases markedly in the range of annealing temperature between 700° and 800°C. The discussion above has shown that the residual surface stresses change little after being annealed at these temperatures. So the increase in σ^* may reflect an increase in the equivalent indentation residual stress, σ_r. This can be explained with the theoretical considerations presented in Section 2:

$$\sigma_r = \frac{Y_r}{Y_a} = \frac{\chi_r}{Y_a}\left(\frac{P}{c^2}\right)\sqrt{\frac{c}{a}} \qquad (14)$$

Since annealing would result in a reduction, rather than increase, in χ_r,[41,42] and both Y_a and c/a are essentially independent of annealing temperature (see Table 3), the decrease in flaw dimension, c, which is caused by flaw healing, should be the only factor for the increase in σ_r.

A continuous decrease in σ^* occurs when annealing temperature increases above 900°C, indicating a rapid relief of the indentation residual stress. However, a significant value of σ^* still remains after being annealed at 1000°C, the limitation of annealing temperature for the present material. It seems to say that annealing may not be an effective method to eliminate the effects of residual stresses in the Knoop-indented bending specimens, at least for the present material.

5 Conclusions

- A detailed theoretical analysis shows that a linear relationship exists between the fracture strength of Knoop indented bending specimen, σ_f, and the inverse square root of the indentation flaw depth, $(1/a)^{1/2}$. The effects of residual stresses can be described properly with the strength revisionary term appearing in the $\sigma_f \sim (1/a)^{1/2}$ fitting equation, while the fracture can be determined directly from the slope term.
- Based on the theoretical consideration, the conventional Knoop-indented bending method for K_{IC} determination is modified. Experimental results show that this modified method may give a reasonable K_{IC} value.
- A limitation for annealing temperature exists above which annealing may result in a change in material properties and/or a serious flaw healing. Therefore, annealing may not be an effective method for eliminating the residual stresses in Knoop-indented bending specimens.

References

1. Evans, A. G. and Charles, E. A., Fracture toughness determinations by indentation. *J. Am. Ceram. Soc.*, 1976, **59**, 371–372.
2. Lawn, B. R., Marshall, D. B., Anstis, G. R. and Dabbs, T. P., Fatigue analysis of brittle materials using indentation flaws: I. *J. Mater. Sci.*, 1981, **16**, 2846–2854.
3. Lawn, B. R., Jakus, K. and Gonzalez, A. C., Sharp vs blunt crack hypotheses in the strength of glass: a critical study using indentation flaws. *J. Am. Ceram. Soc.*, 1985, **68**, 25–34.
4. Laugier, M. T., New formula for indentation toughness in ceramics. *J. Mater. Sci. Lett.*, 1987, **6**, 355–356.
5. Krause, R. F., Rising fracture toughness from the bending strength of indented alumina beams. *J. Am. Ceram. Soc.*, 1988, **71**, 338–343.
6. Marshall, D. B., Controlled flaws in ceramics: a comparison of Knoop and Vickers indentation. *J. Am. Ceram. Soc.*, 1983, **66**, 127–131.
7. Petrovic, J. J., Effect of indenter geometry on controlled-surface-flaw fracture toughness. *J. Am. Ceram. Soc.*, 1983, **66**, 277–283.
8. Lawn, B. R. and Wilshaw, T. R., Indentation fracture: principles and applications. *J. Mater. Sci.*, 1975, **10**, 1049–1081.
9. Marshall, D. B. and Lawn, B. R., Residual stress effects in sharp contact cracking: I, indentation fracture mechanics. *J. Mater. Sci.*, 1979, **14**, 2001–2012.
10. Lawn, B. R., Evans, A. G. and Marshall, D. B., Elastic/plastic indentation damage in ceramics: the median/radial crack system. *J. Am Ceram. Soc.*, 1980, **63**, 574–581.
11. Chiang, S. S., Marshall, D. B. and Evans, A. G., The response of solids to elastic/plastic indentation. *J. Appl. Phys.*, 1982, **53**, 298–317.
12. Marshall, D. B., Geometrical effects in elastic/plastic indentation. *J. Am. Ceram. Soc.*, 1984, **67**, 57–60.
13. Marshall, D. B., Lawn, B. R. and Chantikul, P., Residual stress effects in sharp contact cracking: II, strength degradation. *J. Mater. Sci.*, 1979, **14**, 2225–2235.
14. Chantikul, P., Anstis, G. R., Lawn, B. R. and Marshall, D. B., A critical evaluation of indentation techniques for measuring fracture toughness: II. *J. Am. Ceram. Soc.*, 1981, **64**, 539–543.
15. Cook, R. F., Lawn, B. R. and Anstis, G. R., Fatigue analysis of brittle materials using indentation flaws: II. *J. Mater. Sci.*, 1982, **17**, 1108–1116.
16. Petrovic, J. J. and Jocobson, L. A., Controlled surface-flaws in hot-pressed SiC. *J. Am. Ceram. Soc.*, 1976, **59**, 34–37.
17. Wills, R. R., Mendiratta, M. G. and Petrovic, J. J., Controlled surface-flaw-initiated fracture in reaction-bonded Si_3N_4. *J. Mater. Sci.*, 1976, **11**, 1330–1334.
18. Quinn, G. D. and Quinn, J. B., Slow crack growth in hot-pressed silicon nitride. In *Fracture Mechanics of Ceramic*, Vol. 6, ed. R. C. Bradt, A. G. Evans, D. P. H. Hasselman and F. F. Lange. Plenum, New York, 1983, pp. 603–636.
19. Lange, F. F., James, M. R. and Green, D. J., Determination of residual surface stresses caused by grinding in polycrystalline Al_2O_3. *J. Am. Ceram. Soc.*, 1983, **66**, C–16–C-17.
20. Walls, D., Evans, A. G., Marshall, D. B. and James, M. R., Residual stresses in machined ceramic surfaces. *J. Am. Ceram. Soc.*, 1986, **69**, 44–47.
21. Samuel, R., Chandrasekar, S., Farris, T. N. and Lichit, R., Effect of residual stresses on the fracture of ground ceramics. *J. Am. Ceram. Soc.*, 1989, **72**, 1960–1966.
22. Mendiratta, M. G. and Petrovic, J. J., Slow crack growth from controlled surface flaws in hot-pressed Si_3N_4. *J. Am. Ceram. Soc.*, 1978, **61**, 226–230.
23. Ikeda, K. and Jgaki, H., Effect of surface flaw size on fracture strength of alumina ceramics. *J. Am. Ceram. Soc.*, 1987, **70**, C–29–C-30.
24. Guan, Z. D. and Gong, J. H., Investigation of test reliability in K_{IC} determination with Knoop indented 3-pt bending method. In *Proceedings of the Third International Symposium on Ceramic Materials and Components for Engines*, ed. V. J. Tennery. The American Ceramic Society Inc., Westerville, OH, 1989, pp. 696–700.
25. Gong, J. H. and Guan, Z. D., A modified indented bending method for the determination of fracture toughness of ceramics. *J. Chinese Ceram. Soc.*, 1991, **19**, 226–233.
26. Newman, J. C. and Raju, I. S., An empirical stress-intensity factor equation for the surface crack. *Eng. Fract. Mech.*, 1981, **15**, 185–192.

27. Govila, R. K., Material parameters for life prediction in ceramics. In *Ceramics for High-Performance Applications*, Vol. 3, ed. E. M. Lenoe, R. N. Katz and J. J. Burke. Plenum, New York, 1983, pp. 535–567.
28. Anstis, G. R., Chantikul, P., Lawn, B. R. and Marshall, D. B., A critical evaluation of indentation techniques for measuring fracture toughness, I. *J. Am. Ceram. Soc.*, 1981, **64**, 533–538.
29. Petrovic, J. J., Jacobson, L. A., Talty, P. K. and Vasudevan, A. K., Controlled surface flaw in hot-pressed Si_3N_4. *J. Am. Ceram. Soc.*, 1975, **58**, 113–116.
30. Lankford, J. and Davison, D. L., The crack-initiation threshold in ceramic materials subject to elastic/plastic indentation. *J. Mater. Sci.*, 1979, **14**, 1662–1668.
31. Shetty, D. K., Wright, I. G., Miner, P. N. and Clauer, A. H., Indentation fracture of WC-Co cermets. *J. Mater. Sci.*, 1985, **20**, 1873–1882.
32. Kirchner, H. P. and Issacson, E. D., Residual stresses in hot-pressed Si_3N_4 grooved by single-point grinding. *J. Am. Ceram. Soc.*, 1982, **65**, 55–60.
33. Guan, Z. D., Gong, J. H., Zhao, Y. Y. and Zhao, X. F., The characteristic stress between two kinds of delayed failure for ceramics at elevated temperature. In *Proceedings of the Fourth International Symposium on Ceramic Materials and Components for Engines*, ed. R. Carlsson, T. Johnsson and L. Kahlman. Elsevier Applied Science, London, 1992, pp. 536–543
34. Gong, J. H. and Guan, Z. D., Effect of residual stress due to Knoop indentation on subcritical crack growth behavior in ceramics. In *Fracture Mechanics of Ceramics*, Vol. 9. ed. R. C. Bradt, D. P. H. Hasselman, D. Munz, M. Sakai and V. Ya. Shenvochenko. Plenum, New York, 1992, pp. 569–574.
35. Govila, R. K., Indentation-precracking and double-torsion methods for measuring fracture mechanics parameters in hot-pressed Si_3N_4. *J. Am. Ceram. Soc.*, 1980, **63**, 319–326.
36. Govila, R. K., Phenomenology of fracture in sintered alpha silicon carbide. *J. Mater. Sci.*, 1984, **19**, 2111–2120.
37. Govila, R. K., Fracture phenomenology of a sintered silicon nitride containing oxide additives. *J. Mater. Sci.*, 1988, **23**, 1141–1150.
38. Guan, Z. D. and Sun, G. S., Study on method to determine K_{IC} values of ceramics by chevron-notched 3-pt bending specimens. In *Proceedings of the Third International Symposium on Ceramic Materials and Components for Engines*, ed. V. J. Tennery. The American Ceramic Society Inc., Westerville, OH, 1989, pp. 586–591.
39. Orange, G., Tanaka, H. and Fantozzi, G., Fracture toughness of pressureless sintered SiC: a comparison of K_{IC} measurement methods. *Ceram. Int.*, 1987, **13**, 159–165.
40. Ghosh, A., Jenkins, M. G., White, K. W., Kobayashi, A. S. and Bradt, R. C., Evelated-temperature fracture resistance of a sintered α-silicon carbide. *J. Am. Ceram. Soc.*, 1989, **72**, 242–247.
41. Ritter, J. E., Mahoney, F. M. and Jakus, K., A comparison of Vickers and Knoop indentation in soda-lime glass. In *Fracture Mechanics of Ceramics*, Vol. 8. ed. R. C. Bradt, A. G. Evans, D. P. H. Hasselman and F. F. Lange. Plenum, New York, 1986, pp. 213–223.
42. Ritter, J. E., Jakus, K. and Shi, P., Effect of contact residual stress on proof testing. *J. Am. Ceram. Soc.*, 1988, **71**, 426–429.